

Thermodynamics of C incorporation on Si(100) from *ab initio* calculations

I. N. Remediakis,^{1,2} Efthimios Kaxiras,^{1,3} and P. C. Kelires^{2,3}

¹*Department of Physics and Division of Engineering and Applied Sciences, Harvard University, Cambridge MA 02138*

²*Department of Physics, University of Crete, 71003 Heraklion, Crete, Greece*

³*Institute of Electronic Structure and Laser, Foundation for Research and Technology-Hellas (FORTH), Heraklion, Crete, Greece*

(Dated: November 2, 2018)

We study the thermodynamics of C incorporation on Si(100), a system where strain and chemical effects are both important. Our analysis is based on first-principles atomistic calculations to obtain the important lowest energy structures, and a classical effective Hamiltonian which is employed to represent the long-range strain effects and incorporate the thermodynamic aspects. We determine the equilibrium phase diagram in temperature and C chemical potential, which allows us to predict the mesoscopic structure of the system that should be observed under experimentally relevant conditions.

PACS numbers: 61.66.Dk, 68.35.Rh, 68.35.Bs

Carbon-enriched silicon systems are the focus of current interest as candidates for a material with tailored electronic properties, which is compatible with well-established silicon technology. The tetravalent nature and large band gap in the diamond structure make carbon an ideal candidate for incorporation in Si. However, the solubility of C in Si under thermodynamic equilibrium is extremely low ($\approx 10^{-5}$) due to the huge mismatch in bond length (35%) and bond energy (60%) between C and Si. Non-equilibrium methods, such as molecular beam epitaxy (MBE), that exploit the higher atomic mobility on surfaces, can be used to overcome this obstacle and enhance solubility [1]. As predicted theoretically by Tersoff[2], C solubility is enhanced by several orders of magnitude near the Si(100) surface, especially in sub-surface layers. Osten *et al.* [3] confirmed experimentally this prediction and observed that C atoms diffuse to sub-surface layers above a certain temperature. This finding opened new possibilities for growth of C-rich metastable structures.

The enhanced solubility near the surface has important consequences. The large tensile strain associated with C incorporation in Si has proven a very powerful tool in device engineering: a small amount of C can compensate the Ge-induced tension in pseudomorphic SiGe layers [4, 5, 6], and can also suppress dopant outdiffusion. This idea was recently implemented in a novel heterojunction bipolar transistor [7]. Another interesting effect[8, 9] produced by C incorporation on the Si(100) surface is an unusual change of the surface periodicity after deposition of even a small amount of C ($\approx \frac{1}{8}$ of a mono-layer (ML)): the well-known $c(2 \times 4)$ or $p(2 \times 2)$ reconstructions of the pure Si surface change to a $c(4 \times 4)$ pattern. This is clearly visible in several LEED experiments after ethylene exposure [10, 11], or MBE [8].

The microscopic features of C incorporation in Si are rather well understood. Previous work by the authors [12, 13, 14] revealed an oscillatory C profile driven by

the competition between two factors: the tendency of C atoms to occupy favorable sites which are determined by the reconstruction strain field, and the preferential arrangement of C atoms at certain distances which minimizes the lattice elastic energy. The profile is characterized by enhancement of C content in the first and third layer, depletion in the second and an exponential reduction from the fourth layer and beyond. The favorable C sites are in the third layer between the surface dimers, being under compressive stress [2, 15] and thus suitable for the smaller-sized C atom. The preferential arrangement of two C atoms in the surface layers is at a third nearest-neighbor position, which is also the lowest-energy configuration in the bulk [1]. The interaction of C atoms in first nearest neighbor position is highly repulsive [12]. Moreover, a recent experiment [8] showed that C-C dimers are quite rare in the annealed C-Si(100) surface.

On the other hand, a mesoscopic picture of the surface structure that would link the atomistic features to long-range strain effects, and predict structures for different growth conditions more relevant to experiment, is lacking. Here, we present an approach that closes this gap and is able to determine the equilibrium surface phase diagram. It is based on first-principles atomistic studies, incorporating microscopic strain and polarity effects, which are expected to have a dominant role in the understanding of C incorporation in the host Si lattice. The results are linked to a classical effective Hamiltonian in a Monte Carlo scheme that incorporates strain into the thermodynamic aspects of the problem.

We considered first all possible atomistic configurations likely to have low energies. Guided by previous work, [2, 12, 13, 16] we can establish a set of rules which should be obeyed by low energy configurations of the C-Si(100) system, namely:

- (i) The surface has $c(4 \times 4)$ periodicity.
- (ii) C substitutes Si atoms only in the first (surface) or in the third layer.

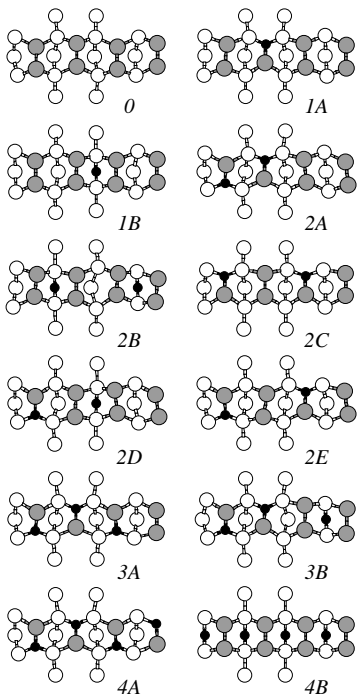


FIG. 1: Top views of the relaxed geometries of the 12 $c(4 \times 4)$ cells we considered. Si surface atoms are shown as grey circles, Si atoms in 2nd and 3rd layers as smaller, white circles, and C atoms as black circles.

(iii) There are no C-C nearest neighbors, or second nearest neighbors.

(iv) Third layer C exists only at sites between pairs of surface dimers.

We constructed every possible structure of the C-Si(100) system, consistent with these rules, with 0, 1, 2, 3 and 4 C atoms per $c(4 \times 4)$ unit cell. These are shown in Fig. 1. The configurations are named nX , n being the number of C atoms in the $c(4 \times 4)$ unit cell and X an index to distinguish structures of the same n .

To study the energetics and the geometrical features of these configurations, we performed *ab initio* DFT/LDA/Pseudopotential calculations [17]. In Table I, we give the energy $E(nX)$ for each configuration nX , relative to the pure Si(100) surface (configuration 0). These energies are defined by:

$$E(nX) = E_{tot}(nX) - n(\mu_C - \mu_{Si}) - E_{tot}(0), \quad (1)$$

where $E_{tot}(nX)$ is the calculated total energy of configuration nX , and μ_C, μ_{Si} are the chemical potentials for C and Si atoms. For Si, the chemical potential is taken to be the energy of the bulk, since this is the natural reservoir for Si atoms due to the presence of steps, terraces, and other surface defects. As a starting point, μ_C is taken to be the energy of a C atom in bulk diamond. We discuss its variation below.

| nX | $E(nX)$ | nX | $E(nX)$ | nX | $E(nX)$ | nX | $E(nX)$ |
|------|---------|------|---------|------|---------|------|---------|
| 1A | 0.19 | 2A | 0.35 | 3A | 1.25 | 4A | 2.31 |
| 1B | 0.08 | 2B | 0.81 | 3B | 1.28 | 4B | 10.39 |
| | | 2C | 1.06 | | | | |
| | | 2D | 0.49 | | | | |
| | | 2E | 0.35 | | | | |

TABLE I: Relative energies for the 12 configurations of Fig. 1, according to Eq. (1) in eV per $c(4 \times 4)$ unit cell. μ_C is taken as the energy of a C atom in diamond. [18]

For low concentration of C, one atom per unit cell, which corresponds to $\frac{1}{8}$ ML coverage, the structure with subsurface C (1B) has lower energy than the one with a Si-C dimer (1A) on the surface. This result is in agreement with experiment: X-ray spectra [10] indicate that for low C deposition, there is almost no C on the surface. A single C atom at a third-layer site relieves the compression due to the surface reconstruction and makes four Si-C bonds while a single C atom on the surface, as part of a dimer, allows the formation of only three SiC bonds. Passing to configurations with more than one subsurface C atom per unit cell, we find that the energy of configuration 2B is considerably higher than that of 2A, 2C, and 2E. Apparently, the presence of two subsurface C atoms per unit cell produces a large distortion of the surrounding Si-Si bonds. Thus, for two C atoms in the unit cell ($\frac{1}{4}$ ML coverage), the best situation is to have both C atoms on the surface. For three C atoms per unit cell ($\frac{3}{8}$ ML coverage), we observe an equivalence of surface/subsurface sites: configurations 3A and 3B have almost the same energy. For the case of four C atoms ($\frac{1}{2}$ ML coverage), there is just one structure (4A) consistent with the rules we discussed before. For illustration purposes, we include another configuration, 4B, containing C atoms in second neighbor positions, which violates rule (iii); its very high energy can be considered as a justification for these rules. We do not go beyond $\frac{1}{2}$ ML coverage because experiments show that this results in disordered structures.

To compare configurations with different C content, we use Eq. (1). This implies that the surface is in equilibrium with a reservoir of C atoms characterized by μ_C . It is generally accepted that C forms small clusters, whose cohesive energies are in the range between -5.5 and -7 eV [19]. In Fig. 2(a), we show the energies of configurations 0, 1B, 2A, 3A and 4A as a function of μ_C . The vertical faint lines denote the transition points at which the preferred structure changes. We observe that the lowest energy structure depends strongly on μ_C and hence on the conditions of C deposition, making it difficult to predict what the actual structure of the system will be. This implies that the equilibrium surface structure might be composed of different configurations at the atomistic

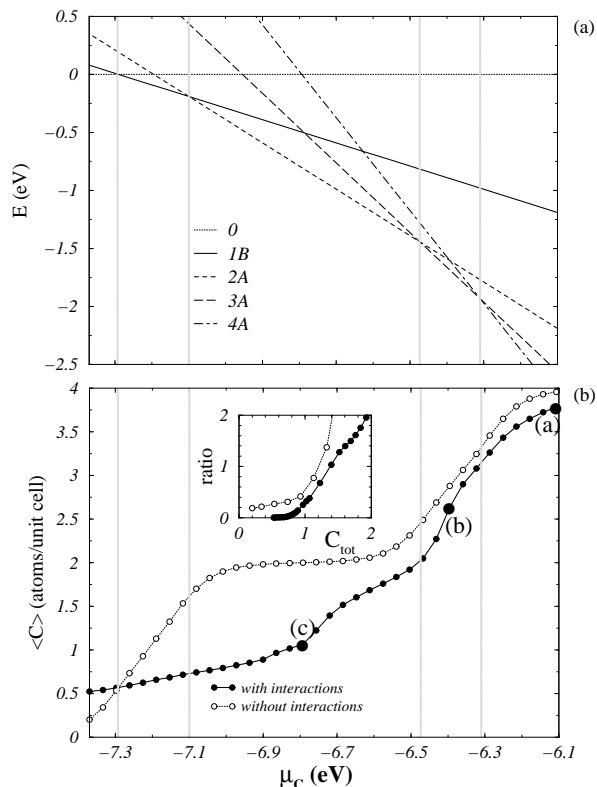


FIG. 2: (a) The energy of the preferred structure for 1,2,3 and 4 C atoms per unit cell as a function of μ_C , from Eq. (1). (b) The average C content of the system as a function of C chemical potential, at 850K, with (filled symbols) and without (open symbols) the elastic strain interactions. The inset shows the ratio of surface to subsurface C atoms at the same temperature, as a function of the total C content in the unit cell. (points marked with bigger symbols correspond to the cases shown in Fig. 3).

level and, consequently, a larger-scale mesoscopic picture is needed. In this picture, the elastic interactions in the boundaries between regions of different C content or atomistic structure will play an important role.

To obtain such a mesoscopic description and study its thermodynamics, we use an effective Hamiltonian within a Monte Carlo scheme. We first construct a classical, 12-state generalized Potts model. We assume that the surface consists of $c(4 \times 4)$ cells, each of which can exist in any of the lowest energy configurations discussed before. The Hamiltonian is

$$\mathcal{H}_{eff} = \sum_{i=1}^N [E(c_i) + \frac{1}{2} \sum_j \Delta E(c_i, c_j)], \quad (2)$$

where the summation on i runs over all N cells, and the summation on j over the 8 nearest neighbors of i (the factor of one half takes into account double-counting of the interaction); c_i is the configuration in cell i , and $\Delta E(c_i, c_j)$ is the interaction energy between the neigh-

boring cells c_i and c_j ($\Delta E(c_i, c_i) \equiv 0$). In order to obtain these interaction energies, we calculated the total energies of all 144 $c(12 \times 12)$ cells consisting of a cell c_i surrounded by 8 c_j cells. These were obtained using Tersoff's empirical potential [20], with a Monte Carlo relaxation method. The key point here is that we are interested in elastic strain interactions between different cells rather than any specific features of their structure; for this type of interaction *between cells* the classical potential employed gives very reasonable results as established by previous studies of similar systems [6, 13]. Having determined \mathcal{H}_{eff} , we performed an equilibrium Monte Carlo study for different values of the temperature and μ_C . We used a 70×70 grid of cells, which was sufficient to get converged averages. For each value of μ_C the system was started from a random configuration at high temperature (1200K) and then was cooled down to room temperature.

In Fig. 2(b) we plot the average total C content of the system as a function of μ_C . The zero for μ_C is taken to be the energy of an isolated C atom. For comparison, we plot the same quantity when the elastic strain interactions, $\Delta E(c_i, c_j)$, are set equal to zero. In both cases the average C content of the system increases with increasing μ_C . The difference between the two curves shows the importance of elastic interactions, which, being of the order of 0.1-0.2 eV/ $c(4 \times 4)$ cell, are more important than the total energy differences in the low μ_C region. This effect weakens as μ_C increases.

Another important consideration, with experimentally observable consequences, is the relative amount of surface versus subsurface C atoms as a function of the total C content C_{tot} in the unit cell, shown in the inset of Fig. 2(b). For larger total C coverage the ratio increases monotonically, approaching infinity as $C_{tot} \rightarrow 4$. Again, we give the case with $\Delta E(c_i, c_j) = 0$ for comparison. There is a critical coverage of 1.39 C atoms per unit cell, or 0.17 ML, beyond which C prefers mostly surface sites. This critical coverage has a weak temperature dependence: it has a maximum around 850K, and then falls monotonically down to roughly 0.16 ML at 300K and 1100K. The increase of the surface C with increasing total C is not unexpected: although third layer compressed sites seem ideal for the smaller C atom, a large amount of subsurface C would cause large strain and raise the total energy dramatically, as exemplified by the case of configuration 4B, which we discussed earlier. From Fig. 2(b) we see that the transition from mostly subsurface to mostly surface C content does not coincide with the change from 1 to 2 C atoms per cell, as suggested by our *ab initio* results, indicating that *the elastic strain interactions play a dominant role in the structure of the surface*.

Representative snapshots of the C distribution from the Monte Carlo run at 850K are shown in Fig. 3. The three cases correspond to the points shown in Fig. 2(a).

An impressive long range order is revealed for the subsurface C (right column of Fig. 3). For low μ_C , Fig. 3(c), this order appears in the form of alternating rows of similar C content. These consist mostly of unit cells corresponding to 0 and $2B$ structures. Although structure $2B$ has relatively high energy, as shown in Table I, a structure of alternating 0 and $2B$ cells seems to be preferable, giving C the chance to take advantage of the desirable third layer compressed sites. The line-pattern is a result of the strong interactions in that range of μ_C , which forces the $c(4 \times 4)$ cells to have the maximum number of different neighbors, 6 for the row pattern and 4 for a chess pattern. The latter pattern is observed for higher μ_C , Fig. 3(b), and is typical for the range of μ_C and temperature corresponding to 1-2 C atoms per unit cell on average (see also Fig 2(b)). In this case, the self-energies of the different configurations dominate over the elastic strain interactions. In the specific example shown in Fig. 3(b), the structure consists mostly of $3A$ and $2B$ cells, at a ratio 2:1. This suggests that for conditions corresponding to this range of μ_C , an alternating pattern of surface/subsurface C is preferable. As μ_C increases the energies of the cells become large enough so that the elastic interactions are not that important, and thus the system does not have much to gain by self-organizing. This results in the random pattern shown in Fig. 3(a), which consists mainly of $4A$ cells with a few $3B$ cells around them. Again, of the two configurations with three C atoms, the one with some subsurface C is preferred when the dominant configuration has all its C atoms on the surface.

Finally, we note that while subsurface C shows this interesting ordering behavior, the surface C seems to be randomly distributed as the patterns of the middle column of Fig. 3 indicate. The ordered structure appearing in the total distribution of C (left column of Fig. 3) is caused by an ordered third-layer C configuration; this is best seen in Fig. 3(c). This idea was implicitly suggested by previous experimental work [8, 10]. From our first-principles calculations, we found that the geometrical features of the Si-Si dimers in all 12 cells are essentially the same. Surface C is invisible, or shows up as a missing Si atom, in STM experiments [16]. This implies that one cannot distinguish, using standard microscopy, between pure Si(100) or Si(100) with vacancies, and a configuration with C in the third layer; the only criterion is the long-range order and the change of the reconstruction.

The work of INR and PCK is supported by a program of the Greek General Secretariat for Research and Technology. EK acknowledges the hospitality of IESL/FORTH where part of this work was completed.

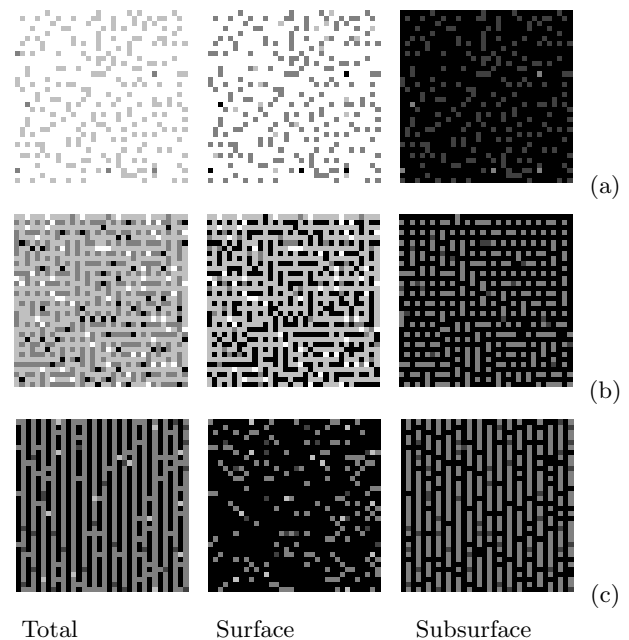


FIG. 3: Density plot of the C distribution on the surface at $T=850K$; (a) $\mu_C = -6.1$, (b) $\mu_C = -6.4eV$, (c) $\mu_C = -6.8$ eV for (c). White corresponds to 4 C atoms, black to 0 C atoms. Each panel represents an area of 38×38 nm² and is $\frac{1}{4}$ of our simulation cell.

-
- [1] H. Rucker, M. Methfessel, E. Bugiel and H. J. Osten Phys. Rev. Lett. **72**, 3578 (1994).
 - [2] J. Tersoff, Phys. Rev. Lett. **74**, 5080 (1995).
 - [3] H. Osten, M. Methfessel, G. Lippert and H. Rucker, Phys. Rev. B **52**, 12179 (1995)
 - [4] K. Eberl, S. S. Iyer, J. C. Tsang, M. X. Goorsky and F. E. LeGoues, J. Vac. Sci. Technol. B **10**, 934 (1992).
 - [5] H. J. Osten, E. Bugiel and P. Zaumseil, Appl. Phys. Lett. **64**, 3440 (1994).
 - [6] P. C. Kelires, Phys. Rev. Lett. **75**, 1114 (1995).
 - [7] H. J. Osten, D. Knoll, B. Heinemann and P. Schley, IEEE Trans. Electron Devices **46**, 1910 (1999).
 - [8] R. Butz and H. Lüth, Surf. Sci **411**, 61 (1998).
 - [9] K. Miki, K. Sakamoto and T. Sakamoto, Appl. Phys. Lett. **71**, 3266 (1997).
 - [10] M. L. Shek, Surf. Sci. **414**, 353 (1998).
 - [11] T. Takaoka, T. Takagaki, Y. Igari and I. Kusunoki, Surf. Sci. **347**, 105 (1996).
 - [12] P. C. Kelires and E. Kaxiras, Phys. Rev. Lett. **78**, 3479 (1997).
 - [13] P. C. Kelires, Surf. Sci. **418**, L62 (1998).
 - [14] P. C. Kelires and E. Kaxiras, J. Vac. Sci. Technol. B, **16**, 1687 (1998).
 - [15] P. C. Kelires and J. Tersoff, Phys. Rev. Lett. **63**, 1164 (1989).
 - [16] O. Leifeld, D. Grützmacher, B. Müller, K. Kern, E. Kaxiras and P. C. Kelires, Phys. Rev. Lett. **82**, 972 (1999).
 - [17] We use a periodic slab of 7 layers terminated by H on one side with 6 layers allowed to relax. We use a plane

wave basis with a cutoff kinetic energy of 36 Ry and the Γ point of the Brillouin zone for reciprocal space sampling. Atomic positions are relaxed until the magnitude of the calculated Hellman-Feynman forces is smaller than 0.001 Ry/a.u. For each configuration, several different starting geometries were considered to ensure that the correct minimum energy structure is found.

[18] To obtain the chemical potentials, we calculate the ener-

gies of C and Si in the diamond structure with the same kinetic energy cutoff and the corresponding k-point grid spacing for the bulk. We use the experimental cohesive energy of diamond, namely 7.37 eV/atom.

[19] R. O. Jones, *J. Chem. Phys.* **110**, 5189 (1999).

[20] J. Tersoff, *Phys. Rev. B* **39**, 5566 (1989).